Eur. Phys. J. D (2020) 74: 155
https://doi.org/10.1140/epjd/e2020-10138-0

THE EUROPEAN PHYSICAL JOURNAL D

Regular Article

The role of spin–orbit effects in the mobility of N^+ ions moving in a helium gas at low temperature[⋆,⋆⋆]

Lamia Aïssaoui[1], Peter J. Knowles[2,a], and Moncef Bouledroua[3]

[1] Laboratoire de Physique des Rayonnements et leurs Interactions avec la Matière, Batna 1 University, Batna 05000, Algeria
[2] School of Chemistry, Cardiff University, Main Building, Park Place, Cardiff CF10 3AT, UK
[3] Laboratoire de Physique des Rayonnements, Badji Mokhtar University, B. P. 12, Annaba 23000, Algeria

Received 5 March 2020 / Received in final form 3 June 2020
Published online 23 July 2020

Abstract. The mobility of N^+ ions in ground-state helium gas at very low temperature is examined with explicit inclusion of spin–orbit coupling effects. The ionic kinetics is treated theoretically with the three-temperature model. The N^+–He interaction potentials, including spin–orbit coupling, are determined using high-level ab initio calculations. Then, the classical and quantal transport cross sections, both needed in the computation of the mobility coefficients, are calculated in terms of the collisional energy of the N^+–He system. The numerical results, at temperature 4.3 K, show the spin–orbit interactions have negligible effect on the mobility coefficients.

1 Introduction

Ion mobility experiments in cooled buffer gases have long been of interest [1]. They are particularly relevant in analytical chemistry, because various large ions can have quite different ion mobilities even if they have the same molar masses. The variations of mobility over wide ranges of gas temperature T and/or electric field strength E serve as excellent probes of the forces between the ions and the atoms or molecules of the gas through which they move. In addition, the mobility data are also needed in laboratory studies of the kinetics of ion-molecule reactions and in applications to the earth's ionosphere [2]. There have been many advances in the kinetic theory of ion mobility, such as the three-temperature (3T) theory [1], and they have now reached the point where the mobility of atomic ions in cooled buffer gases can be calculated with ab-initio methods of higher accuracy than can be measured [3].

By making use of the Gram–Charlier approach [4] and quantum-mechanical transport cross sections, we have computed in a previous paper the C^+ ionic mobility in He gas at the two specific temperatures 4.3 and 77 K [5]. The same mobility has also been examined classically by Tuttle et al. [6] with the inclusion of the spin–orbit (SO) couplings. Both theoretical works have been unable to reproduce the shallow minimum of the mobility coefficient at 4.3 K as measured by Matoba et al. [7]. Such failures incited us to apply both quantal and classical methods to a different system, namely, the open-shell ionic NHe^+ diatom, at $T = 4.3$ K. We use three-temperature theory and the obtain the quantal transport cross sections with the inclusion of the spin–orbit effects to explore theoretically the causes of the unusual behaviour and peculiar shape of the N^+ ion mobility in a cooled buffer gas made exclusively of ground helium at the very low temperature 4.3 K. The results are compared with the measurements of Sanderson et al. [8] obtained with a cooled selected ion drift tube at the temperature 4.35 K. The low-temperature variation of the ion mobility with electric field is found to be particularly sensitive to the various approximations made in its evaluation. We have therefore chosen to compute the ab initio NHe^+ potential-energy curves, including the effects of spin–orbit (SO) couplings, to a controlled high accuracy, as well as investigating the possible effects of using the full quantum-mechanical approximations to the dynamics instead of a classical treatment.

In the following sections, we report the details of the present calculations of the N^+–He interaction potentials that arise from the lowest atomic asymptotes of the open-shell $N^+\left(^3P_J\right) + He\left(^1S_0\right)$ system, the quantal and classical transport cross sections, and the mobility variations with electric strength, as implemented in the Fortran codes PC.F90 and GC.F90 of Viehland [9].

⋆ Electronic Supplementary Information (ESI) available: All the data points derived from the ab initio potentials of the ground N^+–He molecular states, without and with the spin–orbit (SO) effects.

⋆⋆ Supplementary material in the form of one pdf file available from the Journal web page at https://doi.org/10.1140/epjd/e2020-10138-0.

[a] e-mail: KnowlesPJ@Cardiff.ac.uk

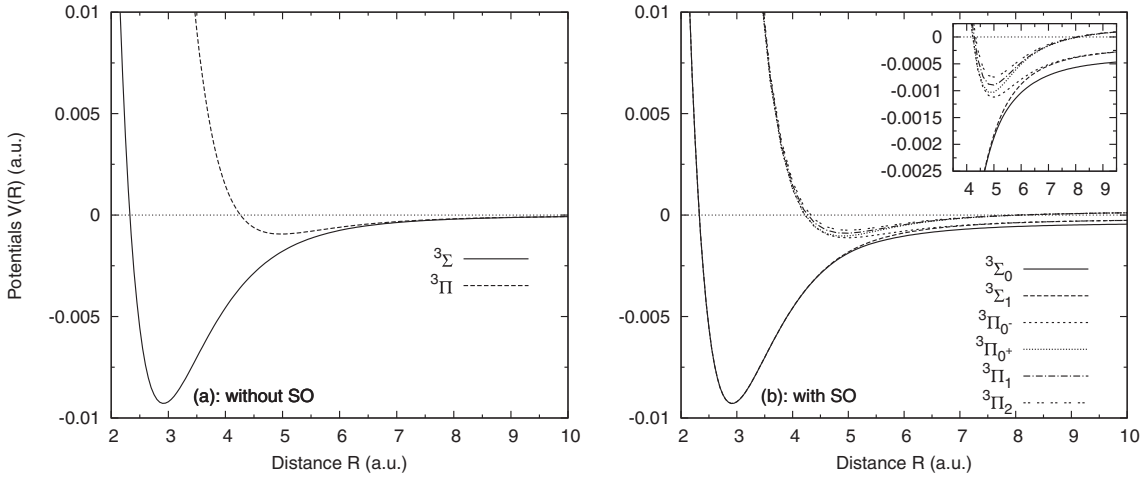

Fig. 1. Interaction potential-energy curves of the ground $N^+\left(^3P\right)$ He state. The dashed lines show the non-SO potentials in (a) while the solid lines show the SO potentials in (b).

Unless otherwise specified, atomic units (a.u.) are used throughout this paper; in particular, energies are given in hartrees (E_h), distances in bohrs (a_0), and $\hbar = 1$.

2 N^+–He interaction potentials

In this section, we describe the ab initio method employed in the generation of the potential-energy curves of the diatomic system correlated with the ground $N^+\left(2s^2 2p^2;\, ^3P\right)$ state that interacts with the ground $He\left(1s^2;\, ^1S\right)$ including the effects of the spin–orbit interactions.

The inclusion of the SO interactions produces three levels from the splitting of the $N^+\left(^3P_J\right)$ state: the lowest state is $^3P_0$, the middle state $^3P_1$ is higher by 48.74 cm^{-1} and the upper state $^3P_2$ is 130.78 cm^{-1} higher [10]. Consequently, the SO interactions lead to the separation of the $^3\Sigma^-$ state into the $^3\Sigma_0^-$ and $^3\Sigma_1^-$ levels, and the $^3\Pi$ state splits into the three distinct levels, namely $^3\Pi_0$, $^3\Pi_1$, and $^3\Pi_2$.

In order to determine the interaction potentials for all the relativistic diatomic states, we first performed non-relativistic calculations for internuclear distances in the range $1.0 \leq R \leq 40.6$ using the spin-restricted open-shell variant of the couple-cluster method with single and double excitations and perturbative treatment of connected triple excitations (RCCSD(T)) [11,12]. In order to accurately represent weak long-range interactions dominated by polarisation effects, we used the doubly-augmented correlation-consistent basis sets [13,14], extrapolating the quadruple- (d-aug-cc-VQZ) and quintuple- (d-aug-cc-V5Z) set correlation energies using the x^{-3} model [15], and applying the standard counterpoise correction for basis-set superposition error [16]. Spin–orbit coupling was then introduced by computing an interaction Hamiltonian using the Breit–Pauli spin–orbit operator and the internally-contracted multireference configuration interaction (MRCI) method [17,18]. All calculations were carried out using the MOLPRO package [19].

The generated data points of the non-SO and SO interaction potentials are displayed in Figures 1a and 1b, respectively and some of their data points are listed in Table 1. All the data points derived from the ab initio potentials of the ground N^+–He molecular states, without and with the spin–orbit (SO) effects, are given in a supplementary material. In particular, the inset in Figure 1b shows the $^3P_0 - ^3P_2$ and $^3P_0 - ^3P_1$ splittings of 123.25 cm^{-1} and 41.08 cm^{-1}, respectively, which are comparable to the experimental values of 130.77 cm^{-1} and 48.74 cm^{-1} [10]. Figure 1b shows that the lowest $^3\Sigma_0^-$ level correlates to $N^+\left(^3P_0\right) + He\left(^1S_0\right)$ asymptote, the $^3\Sigma_1^-$ and $^3\Pi_{0^-}$ levels both correlate to $N^+\left(^3P_1\right) + He\left(^1S_0\right)$ asymptote, and the three highest $^3\Pi_{0^+}$, $^3\Pi_1$, and $^3\Pi_2$ levels correlate to $N^+\left(^3P_1\right) + He\left(^1S_0\right)$ asymptote. It should be noted that $\Omega = -0$ for the $^3\Pi_{0^-}$ level differs from $\Omega = +0$ for the $^3\Pi_{0^+}$ level as obtained in the potentials calculations of Soldàn et al. [20].

In using the generated NHe^+ potentials to compute *quantum-mechanically* the transport cross sections, without or with the SO effects, we slightly altered the data points in order to connect them smoothly with the Born–Mayer and the long-range forms. Indeed, in the short-range region, i.e., $R < 1.0$, the ion-atom curves follow the Born–Mayer relationship [21]

$$V_{\mathrm{SR}}(R) = \alpha \exp(-\beta R), \tag{1}$$

with α and β being two constant parameters. Their values are listed in Table 2. For the long-range region, namely, $R > 40.6$, the extension is chosen of the analytic form [22,23]

$$V_{\mathrm{LR}}(R) = -\frac{C_4}{R^4} - \frac{C_6}{R^6} - \frac{C_8}{R^8}, \tag{2}$$

where C_4 is the dipole–dipole induction coefficient equal to half of the dipole polarizability α_d of the neutral helium atom, and C_6 and C_8 contain contributions from both dispersion and induction. With the basis-set described above, the CI dipole polarizability of He is 1.382; for representing

Table 1. Data points derived from the ab initio potentials of the ground N^+–He molecular states, without and with the spin–orbit (SO) effects. The numbers in the parenthesis indicate powers of 10. All the data are in a.u.

	Without SO		With SO					
R	$^3\Sigma^-$	$^3\Pi$	$^3\Sigma_0^-$	$^3\Sigma_1^-$	$^3\Pi_{0-}$	$^3\Pi_{0+}$	$^3\Pi_1$	$^3\Pi_2$
1.0	+1.1879	+1.8083	+1.1879	+1.1879	+1.8080	+1.8080	+1.8083	+1.8085
1.6	+1.2892 (−1)	+5.8748 (−1)	+1.2892 (−1)	+1.2892 (−1)	+5.8729 (−1)	+5.8729 (−1)	+5.8748 (−1)	+5.8767 (−1)
2.0	+2.5378 (−2)	+2.6863 (−1)	+2.5378 (−2)	+2.5378 (−2)	+2.6850 (−1)	+2.6851 (−1)	+2.6863 (−1)	+2.6876 (−1)
2.6	−7.3860 (−3)	+7.9120 (−2)	−7.3867 (−3)	−7.3864 (−3)	+7.8945 (−2)	+7.8950 (−2)	+7.9121 (−2)	+7.9296 (−2)
3.0	−9.2006 (−3)	+3.2516 (−2)	−9.2022 (−3)	−9.2014 (−3)	+3.2335 (−2)	+3.2337 (−2)	+3.2517 (−2)	+3.2696 (−2)
3.6	−6.4792 (−3)	+6.7638 (−3)	−6.4844 (−3)	−6.4818 (−3)	+6.5800 (−3)	+6.5852 (−3)	+6.7665 (−3)	+6.9478 (−3)
4.0	−4.5681 (−3)	+1.4536 (−3)	−4.5799 (−3)	−4.5799 (−3)	+1.2687 (−3)	+1.2805 (−3)	+1.4593 (−3)	+1.6385 (−3)
4.6	−2.5940 (−3)	−7.5834 (−4)	−2.6349 (−3)	−2.6126 (−3)	−9.4397 (−4)	−9.0305 (−4)	−7.3969 (−4)	−5.7272 (−4)
5.0	−1.7829 (−3)	−9.3473 (−4)	−1.8759 (−3)	−1.8224 (−3)	−1.1217 (−3)	−1.0287 (−3)	−8.9523 (−4)	−7.4772 (−4)
5.6	−1.0497 (−3)	−7.5695 (−4)	−1.2669 (−3)	−1.14101 (−3)	−9.4408 (−4)	−7.2692 (−4)	−6.6568 (−4)	−5.6982 (−4)
6.0	−7.5524 (−4)	−6.0102 (−4)	−1.0370 (−3)	−8.8060 (−4)	−7.8817 (−4)	−5.0645 (−4)	−4.7567 (−4)	−4.1387 (−4)
6.6	−4.8325 (−4)	−4.1451 (−4)	−8.1374 (−4)	−6.3921 (−4)	−6.0169 (−4)	−2.7119 (−4)	−2.5856 (−4)	−2.2734 (−4)
7.0	−3.6897 (−4)	−3.2493 (−4)	−7.1477 (−4)	−5.3543 (−4)	−5.1211 (−4)	−1.6630 (−4)	−1.5847 (−4)	−1.3775 (−4)
7.6	−2.5504 (−4)	−2.2995 (−4)	−6.1294 (−4)	−4.3010 (−4)	−4.1713 (−4)	−5.9231 (−5)	−5.4885 (−5)	−4.2769 (−5)
8.0	−2.0329 (−4)	−1.8534 (−4)	−5.6582 (−4)	−3.8172 (−4)	−3.7252 (−4)	−9.9914 (−6)	−6.9151 (−6)	+1.8396 (−6)
8.6	−1.4823 (−4)	−1.3680 (−4)	−5.1503 (−4)	−3.2979 (−4)	−3.2398 (−4)	+4.2817 (−5)	+4.4756 (−5)	+5.0382 (−5)
9.0	−1.2177 (−4)	−1.1311 (−4)	−4.9040 (−4)	−3.0468 (−4)	−3.0030 (−4)	+6.8334 (−5)	+6.9793 (−5)	+7.4068 (−5)
9.6	−9.2301 (−5)	−8.6452 (−5)	−4.6278 (−4)	−2.7658 (−4)	−2.7364 (−4)	+9.6847 (−5)	+9.7831 (−5)	+1.0073 (−4)
10.0	−7.7554 (−5)	−7.2985 (−5)	−4.4889 (−4)	−2.6247 (−4)	−2.6017 (−4)	+1.1116 (−4)	+1.1193 (−4)	+1.1420 (−4)

Table 2. The adopted short-range parameters, that appear in equation (1), used in the construction of the ground N^+–He potential-energy curves. All the data are in a.u.

	^3P		$^3P_0$	$^3P_1$		$^3P_2$		
Parameters	$^3\Sigma^-$	$^3\Pi$	$^3\Sigma_0^-$	$^3\Sigma_1^-$	$^3\Pi_{0-}$	$^3\Pi_{0+}$	$^3\Pi_1$	$^3\Pi_2$
α	43.825	21.812	43.789	43.807	21.811	21.818	21.815	21.813
β	3.608	2.490	3.607	3.607	2.490	2.491	2.490	2.490

the long-range potentials, we used $\alpha_d = 1.384$ [24], with C_6 and C_8 determined as fitting parameters.

For the *classical* calculations, the Viehland PC.F90 code shifts only the long-range potential at the last data point $R = 40.6$ that agrees with the inverse fourth power term R^{-4} to determine the C_4 coefficients. This accounts for the attraction between the charge on the ion and the dipole induced in the polarized neutral atom. Moreover, at a low gas temperature and for a weak electric field, the mobility is dominated by the leading term that appears in the long-range polarization energy shown in equation (2) and approaches the polarizability limit as the effective temperature tends to zero Kelvin. This mobility limit is expressed at the standard gas density by [1]

$$K_{\rm pol} = \frac{13.853\,{\rm cm}^2\,{\rm V}^{-1}\,{\rm s}^{-1}}{\sqrt{(\alpha_d/4\pi\varepsilon_0)/{\rm \AA}^3\,\mu/{\rm Da}}}, \qquad (3)$$

with μ being the reduced mass of the ion-neutral species.

In order to characterize quantitatively the present constructed potentials, we list in Table 3 the internuclear separations σ for which $V(\sigma) = 0$, as well as the the equilibrium internuclear distance R_e and the potential depth D_e for each diatomic state. The R_e and D_e data sets are both compared with those obtained by Soldàn et al. [20]. They derived these two parameters from RCCSD(T) for non-SO potentials and from unmorphed spin-free potential-energy curves for the SO potentials. The same parameters are also compared with those derived by Buenker et al. [25] from MRD-CI for the SO potentials and by Gu et al. [26] from MRD-CI and Frenking et al. [27] for the non-SO potentials. One may notice that the present determined R_e and D_e values are mostly in good agreement with those of Soldàn et al. [20].

3 Diffusion cross sections

The diffusion or momentum-transfer cross sections Q_d are the key intgermediates between the ion-atom interaction potential and the diffusion or mobility coefficient. The numerical determination of $Q_d(\varepsilon)$ is usually accomplished over wide ranges of the energy ε of the N^+–He relative motion. The collisions are supposed as occurring between two structureless species with the orbital angular momentum quantum numbers $l \geq 0$. In the case of ion-atom elastic collisions, the general expression of $Q_d(\varepsilon)$ is given by the integral [1,28]

$$Q_d(\varepsilon) = 2\pi \int_0^\pi (1 - \cos\theta)\,\sigma(\theta, \varepsilon)\sin\theta d\theta, \qquad (4)$$

Table 3. Selected spectroscopic parameters compared with previous published data. The potential depths D_e are measured with respect to the dissociation limits of the respective ab initio N^+–He molecular states.

	^3P		$^3P_0$	$^3P_1$		$^3P_2$			
Parameters	$^3\Sigma^-$	$^3\Pi$	$^3\Sigma_0^-$	$^3\Sigma_1^-$	$^3\Pi_{0^-}$	$^3\Pi_{0^+}$	$^3\Pi_1$	$^3\Pi_2$	Refs.
σ (Å)	1.23	2.26	1.24	1.23	2.26	2.21	2.23	2.26	This work
R_e (Å)	2.92	4.97	2.92	2.92	4.98	4.90	4.94	4.97	This work
	2.92	4.98	2.92	2.92	4.99	4.90	4.95	4.99	Soldàn et al. [20]
			3.00	3.00	5.10	4.90	5.00	5.10	Buenker et al. [25]
	3.08	5.44							Gu et al. [26]
	3.30								Frenking et al. [27]
D_e (cm^{-1})	2040	205	1956	1997	205	269	238	205	This work
	2006	202	1919	1965	203	296	235	203	Soldàn et al. [20]
			1596	1646	157	226	193	157	Buenker et al. [25]
	1414	31							Gu et al. [26]
	1435								Frenking et al. [27]

where $\sigma(\theta, \varepsilon)$ is the differential cross section for elastic scattering through the angle θ by the ion-atom interaction potential. The $\sigma(\theta, \varepsilon)$ is therefore a tool to determine the *quantal* and *classical* momentum-transfer cross sections.

3.1 Quantal cross sections

For the *quantal* calculation of the diffusion cross sections, equation (4) leads to the relationship [28]

$$Q_d(\kappa) = \frac{4\pi}{\kappa^2} \sum_{l=0}^{\infty} (l+1) \sin^2(\eta_{l+1} - \eta_l), \tag{5}$$

where $\kappa = \sqrt{2\mu\varepsilon}$ is the wave number of the relative motion at energy ε and η_l are the energy-dependent phase shifts. Numerically, the quantal calculations of the phase shifts η_l are performed up to a certain large value of the orbital angular momentum l^* beyond which they are achieved with the semi-classical approximation [28,29]

$$\eta_l \approx -\mu \int_{R_0}^{\infty} \frac{V(R)}{\sqrt{(\kappa R)^2 - (l+1/2)^2}} RdR, \tag{6}$$

where the lower limit R_0 verifies the relationship

$$\kappa R_0 = \left(l + \frac{1}{2}\right). \tag{7}$$

Equation (5) shows the orbiting resonances when the relative energy ε corresponds to a significant increase in the phase shifts η_l.

In Figure 2a, we display the quantal diffusion cross sections corresponding to the non-SO NHe^+ states, $^3\Sigma$ and $^3\Pi$, and to the SO NHe^+ states, $^3\Sigma_0^-$, $^3\Sigma_1^-$, $^3\Pi_{0^-}$, $^3\Pi_{0^+}$, $^3\Pi_1$, and $^3\Pi_2$. It clearly shows that the quantal effects are important at lower energies for the quantum-mechanical cross sections where they exhibit undulations with some regular peaks occurring at the orbiting resonances. One may observe that these orbiting resonances of the diffusion cross sections are strictly related to the energy depth of the interaction potentials and they decrease beyond it.

3.2 Classical cross sections

The *classical* diffusion cross sections are calculated, in this work, by using the Fortran code PC.F90 of Viehland [30]. The general formula of the classical momentum-transfer cross sections is given as [1]

$$Q_d(\varepsilon) = 2\pi \int_0^{\infty} [1 - \cos\theta(b, \varepsilon)] \, bdb, \tag{8}$$

with b being the impact parameter. The angle of deflection θ is defined by

$$\theta(b, \varepsilon) = \pi - 2b \int_{R_0}^{\infty} \left[1 - \frac{b^2}{R^2} - \frac{V(R)}{\varepsilon}\right]^{-1/2} \frac{dR}{R^2}, \tag{9}$$

where the distance of closest approach R_0 is the outermost of

$$1 - \frac{b^2}{R^2} - \frac{V(R_0)}{\varepsilon} = 0. \tag{10}$$

The results of the classical momentum-transfer cross sections for the non-SO and SO NHe^+ states are both plotted in Figure 2b.

3.3 Average cross sections

Since the actual ionic state populations are not definitely known, one need to compute the *average* diffusion cross sections. These are generally given by the statistically weighted formula [7]

$$\overline{Q}_d = \frac{\sum_j g_j Q_d^j}{\sum_j g_j}, \tag{11}$$

where g_j is the multiplicity of the considered molecular state j and Q_d^j is the corresponding diffusion cross section.

Hence, the average cross sections $\overline{Q}_d$ for the triplet non-SO states $^3\Sigma^-$ and $^3\Pi$ are given by the weighted sum [1]

$$\overline{Q}_d = \frac{1}{3} Q_d^{\Sigma} + \frac{2}{3} Q_d^{\Pi}. \tag{12}$$

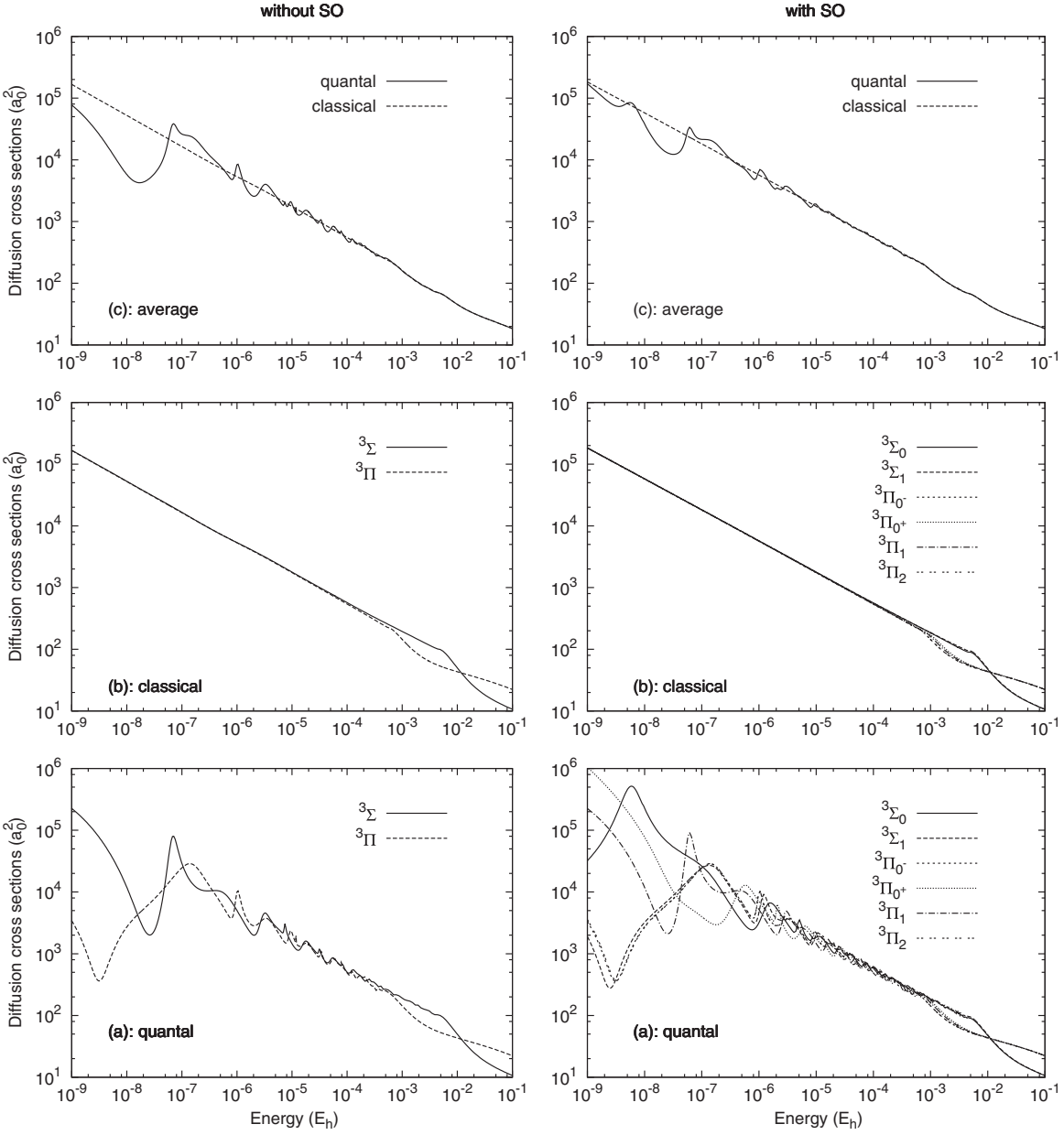

Fig. 2. Diffusion cross sections varying with energy. The left side presents the non-SO diffusion cross sections and the right side presents the SO ones. The individual quantal cross sections are shown/presented/plotted in (a), the individual classical cross sections in (b), and the average cross sections in (c).

In the relativistic case, the average cross section $\overline{Q}_d$ for the triplet-SO $N^+\left(^3P_J\right)$–He state is calculated from a $(1:3:5)$ mix of the cross-sections for the $^3P_0$, $^3P_1$, and $^3P_2$ levels respectively; however these are further broken down as $^3P_1$ contributions coming from a $(2:1)$ mix of those from the $^3\Sigma_1$ and $^3\Pi_{0^-}$ levels, and $^3P_2$ from a $(1:2:2)$ mix of $^3\Pi_{0^+}$, $^3\Pi_1$ and $^3\Pi_2$ levels. To show the difference between the two calculation methods, we compare in Figure 2c between the average quantum-mechanical and classical momentum-transfer cross sections, which reveals the absence of the orbiting resonances in the classical calculation for the energies below 10^{-3}.

4 Mobility results and discussion

In this section, we employ the obtained results of the average quantal and classical transport cross sections to compute the corresponding reduced mobility coefficients K_0 of $N^+\left(^3P_J\right)$ in He as a function of the ratio E/N of the electric field strength to the gas number density at temperature 4.3 K and also as a function of the effective temperature T_{eff} defined as [1]:

$$\frac{3}{2}k_BT_{\text{eff}} = \frac{3}{2}k_BT + \frac{1}{2}Mv_d{}^2, \tag{13}$$

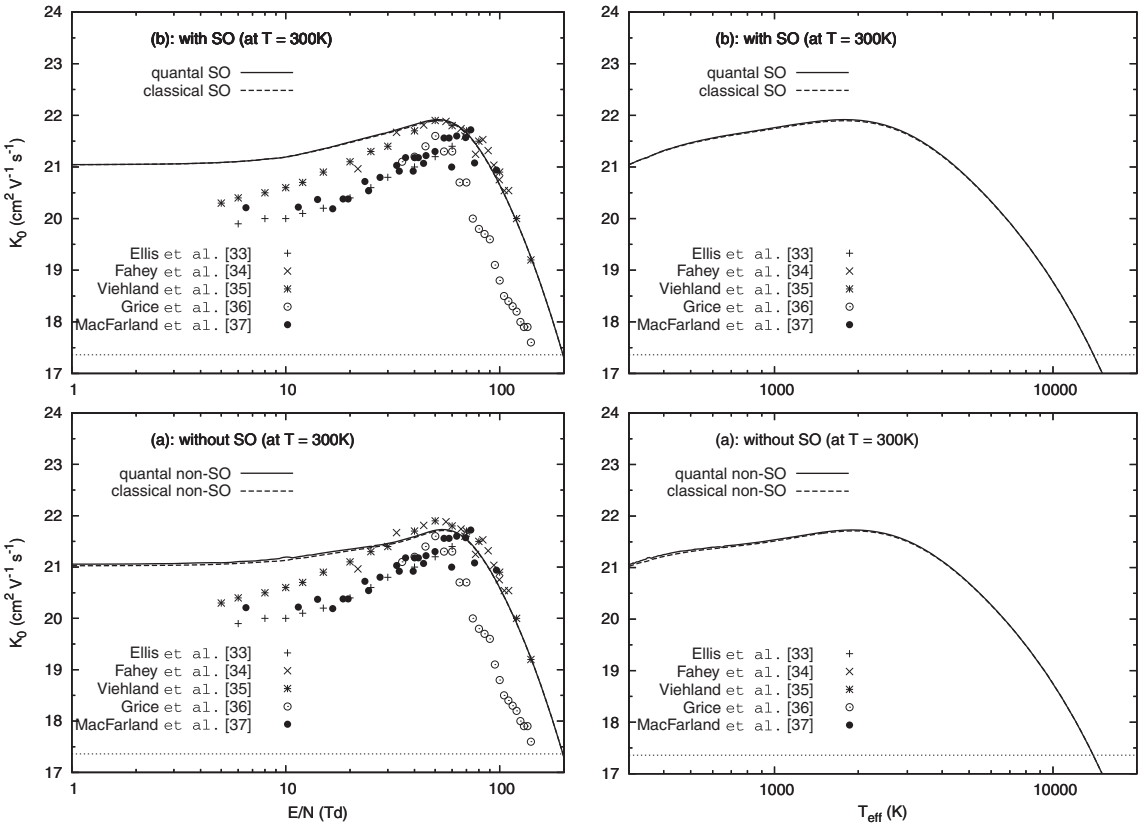

Fig. 3. Comparison of quantal non zero-field mobilities of the $N^+ ({}^3P)$ ions in He as a function of E/N (left side) and as a function of $T_{\rm eff}$ (right side) at $T \approx 300\,\mathrm{K}$, with those obtained classically. The symbols are experimental values from Ellis et al. [33], Fahey et al. [34], Viehland et al. [35], Grice et al. [36] and McFarland et al. [37]. The horizontal dotted lines represent the polarization limit $K_{\rm pol} = 17.34\,\mathrm{cm^2\,V^{-1}\,s^{-1}}$.

where $T_{\rm eff}$ characterizes the kinetic energy of an ion-neutral gas collision in the centre-of-mass frame, M is the neutral gas mass, v_d is the ion drift velocity and $k_{\rm B}$ is the Boltzmann's constant. The calculations are performed with the Fortran code GC.F90 [9], which relies on the Gram–Charlier series [4] and uses the matrix elements of the three-temperature theory of gaseous ion transport [31,32]. The details of the numerical computations are very similar to those described in our previous CHe^+ paper [5] and in Tuttle et al. [6].

In order to test the reliability and consistency of the present interaction potentials, we have first of all chosen to compute the reduced mobility coefficients of N^+ in He at room temperature, namely at $T \simeq 300\,\mathrm{K}$. The obtained results of the quantum-mechanical and classical mobilities, as a function of the ratio E/N and as a function of $T_{\rm eff}$, are shown in Figure 3. They are also compared in the same plot with the experimental measurements of Ellis et al. [33] at 300 K, of Fahey et al. [34] and Viehland et al. [35] at 299 K, of Grice et al. [36] at 298 K, and of McFarland et al. [37] at 297 K. At room temperature, both quantal and classical methods produced the same mobility values that are in a very good agreement with the experimental data of Fahey et al. [34] and Viehland et al. [35], The concordance is mainly observed for $E/N \geq 10\,\mathrm{Td}$, where $1\,\mathrm{Td} = 10^{-21}\,\mathrm{Vm^2}$. Moreover, as Figures 3a and 3b clearly displays, the reduced mobility coefficients based on quantal and classical potential-energy curves, SO effects included, approach at very weak E/N the value $21.04\,\mathrm{cm^2\,V^{-1}\,s^{-1}}$. As the electric field increases in intensity, the present $N^+ ({}^3P)$ mobility results reach a maximum values that lie between 40 and 60 Td, which are believed typical for mobilities of light ions in helium [34,35]. In addition, as already emphasized by Fahey et al. [34], the *zero*-field mobilities in He show they are, in general, substantially different from the polarization limit $K_{\rm pol} = 17.34\,\mathrm{cm^2\,V^{-1}\,s^{-1}}$ [33]. This fact indicates that, for ions at room temperatures, the Langevin approximation [1] is poor for the weakly-polarisable helium. Theoretically, the polarization limit is attained when the electric field and the gas temperature are low enough, i.e., $(E \longrightarrow 0)$ and $(T \longrightarrow 0)$ [1].

Being satisfied with the generated results at room temperature, all the quantal and classical calculations of the reduced mobilities, with and without SO effects, in connection with the diffusion of the ground $N^+ ({}^3P_J)$ ions in helium gas at 4.3 K are displayed in Figures 4a and 4b. They are also contrasted with some experimental and published data. The non-SO values at the same temperature have been computed quantum-mechanically by Lias et al. [38]. They are presented in Figure 4a. At lower E/N, the N^+ ion mobility values approach the polarization limit

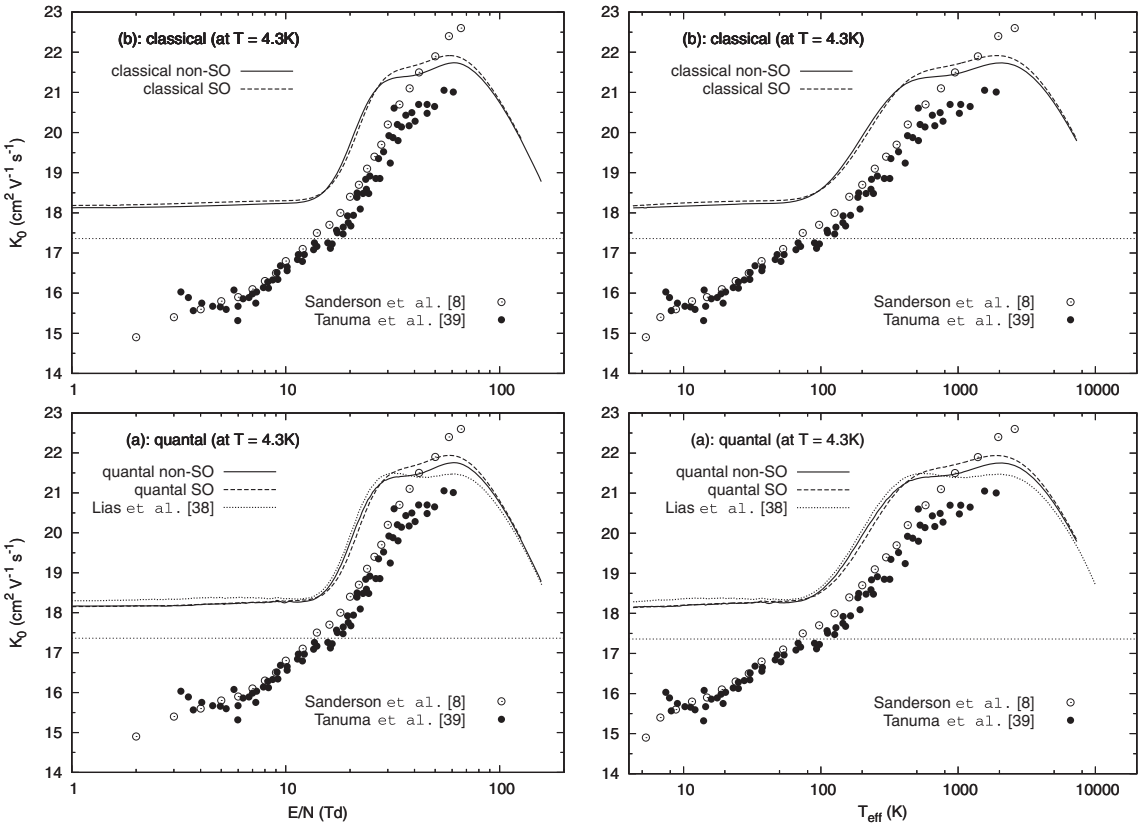

Fig. 4. Quantal and classical non zero-field mobilities of $N^+\left({}^3P\right)$ ions in He as a function of E/N (left side) and as a function of $T_{\rm eff}$ (right side) at $T = 4.3\,\mathrm{K}$. They are compared with the experimental values from Sanderson et al. [8] and Tanuma et al. [39]. The horizontal dotted lines represent the polarization limit $K_{\rm pol} = 17.34\,\mathrm{cm^2\,V^{-1}\,s^{-1}}$.

$K_{\rm pol} \simeq 17.34\,\mathrm{cm^2\,V^{-1}\,s^{-1}}$. Beyond, the present calculations yield, at the particular $E/N = 2\,\mathrm{Td}$, the reduced mobilities 18.1 and $18.2\,\mathrm{cm^2\,V^{-1}\,s^{-1}}$, without and with SO effects, respectively. The former value is comparable with the recommended value $14.9 \pm 0.3\,\mathrm{cm^2\,V^{-1}\,s^{-1}}$ of Sanderson et al. [8]. One may further observe from Figure 4 that both theoretical and experimental mobilities, either without or with the spin–orbit effects, have the expected shapes in intermediate and higher electric fields. This behaviour is completely absent with the Sanderson et al. results [8], which rather show monotonically increasing values.

On the other hand, the impact of the spin–orbit couplings may be evaluated by looking particularly at the zero-field limit. Table 4 lists the zero-field results of the diffusion and reduced mobility coefficients at two different temperatures, 4.3 and 300 K, with and without the SO interactions. The present results are compared with the available published data. They show, in particular, a decrease in the numerical results mainly at the higher temperature when the spin–orbit effects are included.

As with the CHe^+ system [5], the present quantal calculations have also been unable to reproduce the shallow minimum found experimentally by Tanuma et al. [39] around $(E/N) \approx 5\,\mathrm{Td}$. As explained by Mason and McDaniel [1] and Matoba et al. [7], this shallow minimum should come from the attractive long-range potential, and the quantum-mechanical orbiting resonances which occur at weak collisional energy. We display in Figures 5a and 5b a comparison of N^+ ion mobilities derived from the use of the average diffusion cross sections with those obtained from the diffusion cross sections of ${}^3P_0$, ${}^3P_1$, and ${}^3P_2$ states. For ${}^3P_0$, both quantal and classical mobility results display a minimum around 50 Td that appears unrelated to the shallow minimum of experimental data around 5 Td; the ${}^3P_1$ and ${}^3P_2$ cross sections show quite different behaviour. It has been argued by Matoba et al. [7] that calculations of the mobility of the $C^+\left({}^2P\right)$ ion in He gas at 4.3 K might show a mobility minimum if the cross sections were computed quantum-mechanically (occurring of the orbiting resonances at low energy), rather than by using the classical-mechanical. Nevertheless, the quantal study of CHe^+ system [5] did not find this minimum; consequently, it seems unlikely that it could be present here.

This discrepancy between theory and experiment remains at present unresolved. One could speculate that the experimental measurements of Sanderson et al. [8], and Tanuma et al. [39], realized with the same drift-tube, are unreliable. Tuttle et al. [6] suggest that for the mobility of $C^+\left({}^2P\right)$ in helium gas at 4.3 K i.e., the complexation of the light ion with He during the drift region followed by rapid collisional break-up could lead to a slight slowing of the passage of ion down the drift tube, and hence to lower mobilities.

Table 4. Zero-field reduced mobility K_0 and diffusion coefficients D at $T = 4.3\,\mathrm{K}$ and room temperature $T = 300\,\mathrm{K}$. The diffusion coefficients are given as D times the pressure $p = 0.250$ torr and the gas density N.

Coefficients		$T = 4.3\,\mathrm{K}$	$T = 300\,\mathrm{K}$	Refs.
$pD\ (\mathrm{cm^2\,Torrs^{-1}})$	Without SO	0.082	462.6	This work
	With SO	0.082	457.2	
			432.0	Fahey et al. [34]
$ND\ (10^{19}\,\mathrm{cm^{-1}\,s^{-1}})$	Without SO	0.018	1.489	This work
	With SO	0.018	1.495	
			1.462	Fahey et al. [34]
$K_0\ (\mathrm{cm^2\,V^{-1}\,s^{-1}})$	Without SO	18.16	21.05	This work
	With SO	18.14	21.04	
			20.50 ± 1.00	Fahey et al. [34]
			20.00 ± 1.20	McFarland et al. [37]

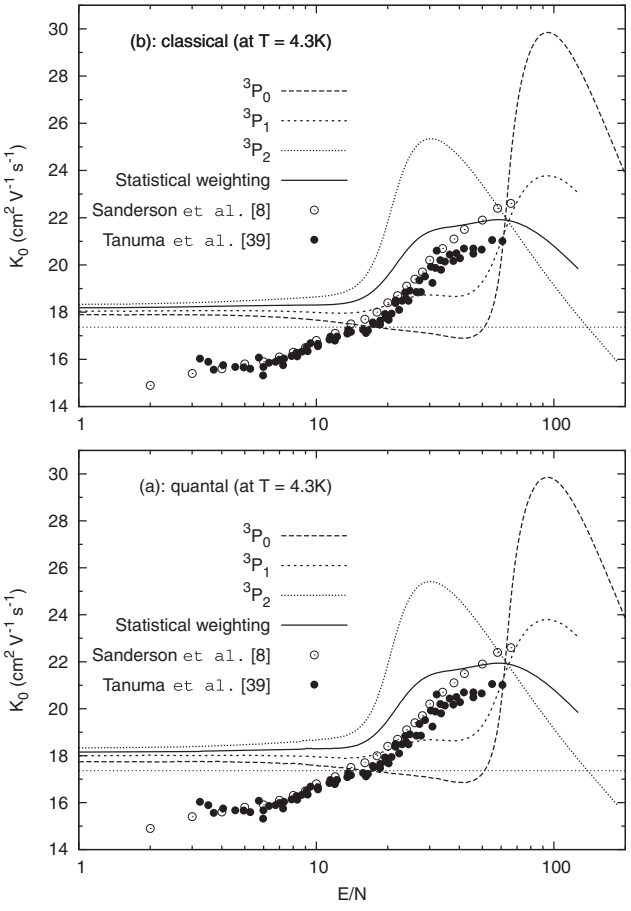

Fig. 5. State contributions to quantal and classical non zero-field mobilities of $N^+\ (^3P)$ ions in He as a function of E/N at $T = 4.3\,\mathrm{K}$. They are compared with the experimental values from Sanderson et al. [8] and Tanuma et al. [39]. The horizontal dotted lines represent the polarization limit $K_{\mathrm{pol}} = 17.34\,\mathrm{cm^2\,V^{-1}\,s^{-1}}$.

5 Conclusion

In this work, the mobility coefficients of N^+ ions moving in a ground buffer gas made of helium have been computed using high-level ab initio methods, both with and without the inclusion of spin–orbit coupling, together with both quantum-mechanical and semiclassical computations of momentum-transfer cross sections and their behaviour with energy. Furthermore, within the Gram–Charlier approach, the coefficients of mobility at 4.3 K and their variation with the ratio E/N of the electric field strength to the gas number density of helium have been analyzed. The calculations show that there is only a very small sensitivity to the spin–orbit interaction, and that its introduction does not reproduce the experimentally observed low mobility at low field strengths.

The authors are very grateful to Dr. K. Alioua for his constructive comments. Special thanks are sent, mainly from M.B., to Dr. Larry A. Viehland, from Chatham University, Pittsburgh, PA, USA, for providing his Fortran codes PC.F90 and GC.F90. The latter program has been used in the main parts of the present calculations.

Author contribution statement

Lamia Aïssaoui and Moncef Bouledroua computed the quantum and classical transport cross sections and transport coefficients. Lamia Aïssaoui and Peter Knowles designed and carried out the electronic structure computations, and wrote the first draft of the manuscript. All authors contributed to the final version of the manuscript.

Publisher's Note The EPJ Publishers remain neutral with regard to jurisdictional claims in published maps and institutional affiliations.

References

1. E.A. Mason, E.W. McDaniel, *Transport Properties of Ions in Gases* (John-Wiley, New York, 1988)

2. S.A. Haider, M.A. Abdu, I.S. Batista, J.H. Sobral, X. Luan, E. Kallio, W.C. Maguire, M.I. Verigin, V. Singh, J. Geophys. Res. **114**, A03311 (2009)
3. L.A. Viehland, T. Skaist, C. Adhikari, W.F. Siems, Int. J. Ion Mobility Spectrom. **20**, 1 (2016)
4. L.A. Viehland, Chem. Phys. **179**, 71 (1994)
5. L. Aïssaoui, M. Bouledroua, K. Alioua, Mol. Phys. **113**, 3740 (2015)
6. W.D. Tuttle, R.L. Thorington, L.A. Viehland, T.G. Wright, Mol. Phys. **113**, 3767 (2015)
7. S. Matoba, H. Tanuma, K. Ohtsuki, J. Phys. B **41**, 145205 (2008)
8. J. Sanderson, H. Tanuma, N. Kobayashi, Y. Kaneko, J. Chem. Phys. **103**, 7098 (1995)
9. A. Yousef, S. Shrestha, L.A. Viehland, E.P.F. Lee, B.R. Gray, V.L. Ayles, T.G. Wright, W.H. Breckenridge, J. Chem. Phys. **127**, 154309 (2007)
10. http://www.nist.gov
11. P.J. Knowles, C. Hampel, H.-J. Werner, J. Chem. Phys. **99**, 5219 (1993)
12. P.J. Knowles, C. Hampel, H.-J. Werner, J. Chem. Phys. **112**, 3106 (2000)
13. T.H. Dunning, Jr., J. Chem. Phys. **90**, 1007 (1989)
14. D.E. Woon, T.H. Dunning, Jr., J. Chem. Phys. **100**, 2975 (1994)
15. A. Halkier, T. Helgaker, P. Jørgensen, W. Klopper, J. Olsen, Chem. Phys. Lett. **302**, 437 (1999)
16. S.F. Boys, F. Bernardi, Mol. Phys. **100**, 65 (1970)
17. H.-J. Werner, P.J. Knowles, J. Chem. Phys. **89**, 5803 (1988)
18. A. Berning, M. Schweizer, H.-J. Werner, P. Knowles, P. Palmieri, Mol. Phys. **98**, 1823 (2000)
19. H.-J. Werner, P.J. Knowles, G. Knizia, F.R. Manby, M. Schütz, Wiley Interdiscip. Rev. Comput. Mol. Sci. **2**, 242 (2012)
20. P. Soldàn, J.M. Hutson, J. Chem. Phys. **117**, 3109 (2002)
21. H. Pauly, in *Atom-Molecule Collision Theory*, edited by R.B. Bernstein (Plenum Press, New York, 1979)
22. R. Côté, A. Dalgarno, Phys. Rev. A **62**, 012709 (2000)
23. F. Bouchelaghem, M. Bouledroua, Phys. Chem. Chem. Phys. **16**, 1875 (2014)
24. G. Łach, B. Jeziorski, K. Szalewicz, Phys. Rev. Lett. **92**, 233001 (2004)
25. R.J. Buenker, J.P. Gu (unpublished results)
26. J.-P. Gu, R.J. Buenker, G. Hirsch, J. Chem. Phys. **102**, 7540 (1995)
27. G. Frenking, W. Koch, D. Cremer, J. Gauss, J.F. Liebman, J. Phys. Chem. **93**, 3397 (1989)
28. N.F. Mott, H.S.W. Massey, *The Theory of Atomic Collisions* (Oxford University Press, Oxford, 1965)
29. A. Dalgarno, M.R.C. McDowell, A. Williams, Philos. Trans. R. Soc. London A **250**, 411 (1958)
30. L.A. Viehland, Y. Chang, Comput. Phys. Commun. **181**, 1687 (2010)
31. S.L. Lin, L.A. Viehland, E.A. Mason, Chem. Phys. **37**, 411 (1979)
32. L.A. Viehland, S.L. Lin, Chem. Phys. **43**, 135 (1979)
33. H.W. Ellis, R.I. Pay, E.W. McDaniel, L.A. Viehland, E.A. Mason, At. Data Nucl. Data Tables **17**, 177 (1976)
34. D.W. Fahey, F.C. Fehsenfeld, D.L. Albritton, J. Chem. Phys. **74**, 2080 (1981)
35. L.A. Viehland, E.A. Mason, At. Data Nucl. Data Tables **60**, 35 (1995)
36. S.T. Grice, P.W. Harland, J.A. Harrison, R.G. A.R. Maclagan, R.W. Simpson, Int. J. Mass Spectrom. Ion Processes **107**, 215 (1991)
37. M. McFarland, D.L. Albritton, F.C. Fehsefeld, E.E. Ferguson, A.L. Schmeltekopf, J. Chem. Phys. **59**, 6610 (1973)
38. S. Lias, L. Aïssaoui, M. Bouledroua, K. Alioua, Mol. Phys. **118**, e1657601 (2020)
39. H. Tanuma, S. Matoba (unpublished results)